THE JOURNAL OF PHYSICAL CHEMISTRY A

Article

pubs.acs.org/JPCA

Quantification of the Keto-Hydroperoxide ($HOOCH_2OCHO$) and Other Elusive Intermediates during Low-Temperature Oxidation of Dimethyl Ether

Kai Moshammer,[†,#] Ahren W. Jasper,[†] Denisia M. Popolan-Vaida,[‡] Zhandong Wang,[§] Vijai Shankar Bhavani Shankar,[§] Lena Ruwe,[∥] Craig A. Taatjes,[†] Philippe Dagaut,[⊥] and Nils Hansen*[,†]

[†]Combustion Research Facility, Sandia National Laboratories, Livermore, California 94551, United States

[‡]Department of Chemistry, University of California—Berkeley, and Chemical Sciences Division, Lawrence Berkeley National Laboratory, Berkeley, California 94720, United States

[§]King Abdullah University of Science and Technology (KAUST), Clean Combustion Research Center (CCRC), Thuwal 23955-6900, Saudi Arabia

[∥]Department of Chemistry, Bielefeld University, D-33615 Bielefeld, Germany

[⊥]Centre National de la Recherche Scientifique (CNRS-INSIS), ICARE, 45071 Orléans Cedex 2, France

Supporting Information

ABSTRACT: This work provides new temperature-dependent mole fractions of elusive intermediates relevant to the low-temperature oxidation of dimethyl ether (DME). It extends the previous study of Moshammer et al. [*J. Phys. Chem. A* **2015**, *119*, 7361−7374] in which a combination of a jet-stirred reactor and molecular beam mass spectrometry with single-photon ionization via tunable synchrotron-generated vacuum-ultraviolet radiation was used to identify (but not quantify) several highly oxygenated species. Here, temperature-dependent concentration profiles of 17 components were determined in the range of 450−1000 K and compared to up-to-date kinetic modeling results. Special emphasis is paid toward the validation and application of a theoretical method for predicting photoionization cross sections that are hard to obtain experimentally but essential to turn mass spectral data into mole fraction profiles. The presented approach enabled the quantification of the hydroperoxymethyl formate ($HOOCH_2OCH_2O$), which is a key intermediate in the low-temperature oxidation of DME. The quantification of this keto-hydroperoxide together with the temperature-dependent concentration profiles of other intermediates including H_2O_2, HCOOH, CH_3OCHO, and CH_3OOH reveals new opportunities for the development of a next-generation DME combustion chemistry mechanism.

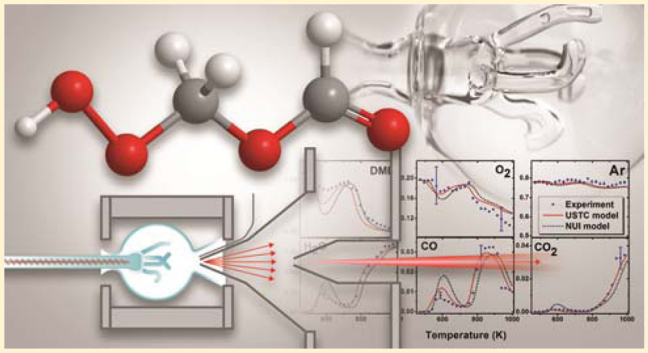

1. INTRODUCTION

Combustion strategies are currently actively explored that offer better efficiency and reduced CO_2 emissions than conventional high-temperature processes while simultaneously decreasing NO_x and soot formation.[1] In this context dimethyl ether (DME, CH_3OCH_3) is an interesting alternative fuel because it has a high cetane number (≥55) and its combustion produces very low gaseous and particulate emissions.[2,3] These properties make DME an ideal alternative fuel to diesel in most compression ignition engines.[4] Low-temperature combustion (LTC) strategies also provide a path toward cleaner combustion, and therefore it is not surprising that many experimental, theoretical, and modeling studies have been carried out to characterize the low-temperature combustion of DME (for recent overviews, see refs 5 and 6).

The fundamentals of the combustion chemistry in the low-temperature regime have been known for decades.[7−9] The chemistry consists of initiation via hydrogen abstraction, followed by additions of molecular oxygen and isomerization and/or fragmentations leading to many partially oxidized intermediates, including keto-hydroperoxides and other peroxy species. The rates and products of each of these steps can vary sensitively with temperature and pressure, and detailed chemical kinetic mechanisms have been developed to model this chemistry.

To develop and validate low temperature oxidation mechanisms and because it has been observed that competing

Received: July 1, 2016
Revised: September 9, 2016
Published: September 17, 2016

DOI: 10.1021/acs.jpca.6b06634
J. Phys. Chem. A 2016, 120, 7890−7901

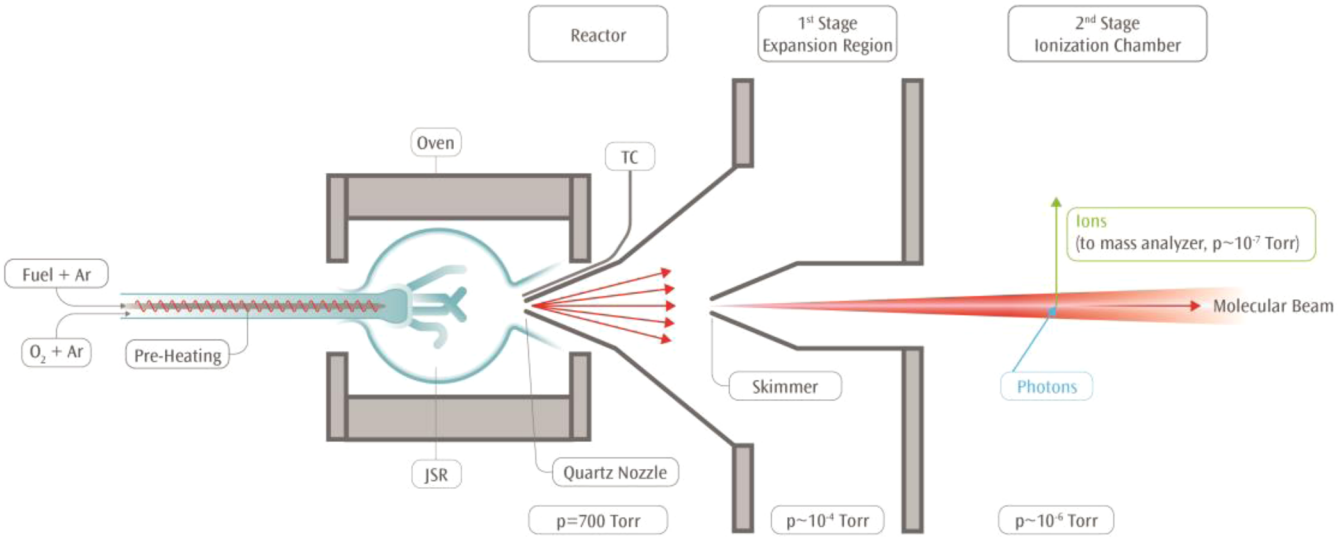

Figure 1. Schematic representation of the experimental setup.

mechanisms can provide similarly accurate predictions for many species despite significantly different incorporated chemistry,[10] it is necessary to sensitively probe the underlying chemistry. To this end, it would be particularly helpful to avail information about mole fraction profiles from key intermediates, such as the keto-hydroperoxides. This class of intermediates is known to be characteristic of low-temperature oxidation chemistry and plays a key role in controlling chain branching, and therefore the knowledge about their concentration is crucial for mechanism developments. However, keto-hydroperoxides were only recently qualitatively detected in experiments that combine jet-stirred reactors (JSR) with molecular beam sampling capabilities and mass spectrometers that employ synchrotron-generated vacuum-ultraviolet radiation for single-photon ionization.[6,11−13] Specifically for DME, the low-temperature oxidation (400−700 K) of dimethyl ether was studied in a jet-stirred reactor using molecular-beam mass spectrometry (MBMS), and the detection and identification of the keto-hydroperoxide hydroperoxymethyl formate (HPMF, HOO-CH_2OCHO) were reported in a recent study that included the present authors.[6]

However, the described detection and identification of elusive intermediates[6,11] can only provide initial guidance for testing the predictive capabilities of chemically detailed mechanisms for low-temperature combustion and for understanding the underlying chemistry. It was mentioned above that more powerful validation targets become available to test the accuracies of the model predictions if reliable quantitative information about these elusive intermediates can be extracted from the experimental data. To extract such crucial information from the above-mentioned photoionization mass spectrometric experiments,[6,11−13] the absolute photoionization cross sections (PICS) of the intermediates need to be known reliably.

For a variety of species PICS have been measured,[14] but PICS are typically not available for highly reactive, short-lived species like the keto-hydroperoxides. Unknown cross sections are sometimes estimated (for example, based on cross sections for similar species or using group additivity rules),[15,16] but the accuracy of these estimates is not reliably known. As a consequence, when species concentrations quantified using estimated cross sections are compared with the results of chemical modeling, it is not clear whether any discrepancies that arise are due to inaccurate estimates of the PICS, errors in the chemistry of the detailed mechanisms, or both. In this paper we describe a theoretical approach to calculate unknown PICS of intermediates that appear in low-temperature oxidation processes.

We first validate the theoretical approach via comparisons with several measured absolute cross sections.[17] The results of this study allow us to quantify the accuracy of the theoretical cross sections to be approximately a factor of 2. Complications that arise in this analysis due to poor Franck−Condon overlaps, excited electronic states of the photoionized cation, and fragmentation of the cation are considered. Subsequently, this theoretical work is combined with the results of ref 6 to report reliable mole fraction profiles as a function of the temperature for the previously identified CH_3OOH and HPMF. In order to give a more complete data set, a total of 15 reactants, products, and intermediates (including key intermediates like H_2O_2, HCOOH, and CH_3OCHO) were also quantified. The new mole fraction profiles are then compared to model predictions using the most widely validated and accepted detailed chemical kinetic mechanisms for DME oxidation,[5,18,19] to illustrate their capabilities and possibilities for an improved description of DME's low-temperature chemistry.

2. EXPERIMENTAL DETAILS AND DATA EVALUATION

2.1. Experimental Details. The experimental work was performed at the Chemical Dynamics Beamline of the Advanced Light Source at the Lawrence Berkeley National Laboratory (LBNL). A jet-stirred reactor (JSR) was coupled to a high-resolution time-of-flight molecular-beam mass spectrometer that relies on single-photon ionization by tunable synchrotron-generated vacuum ultraviolet (VUV) radiation. Figure 1 shows a schematic representation of the experimental setup. The apparatus consists of a jet-stirred reactor and a two-stage differentially pumped vacuum chamber that hosts the ion source of the mass spectrometer. The reaction gases are sampled out of the jet-stirred reactor via a quartz nozzle with a ~50 μm orifice diameter at the tip which is located in the exit of the reactor. An electrically heated oven completely encloses the reactor and allows for adjusting its temperature over the desired range. This assembly is surrounded by a water-cooled stainless steel chamber.

DOI: 10.1021/acs.jpca.6b06634
J. Phys. Chem. A 2016, 120, 7890−7901

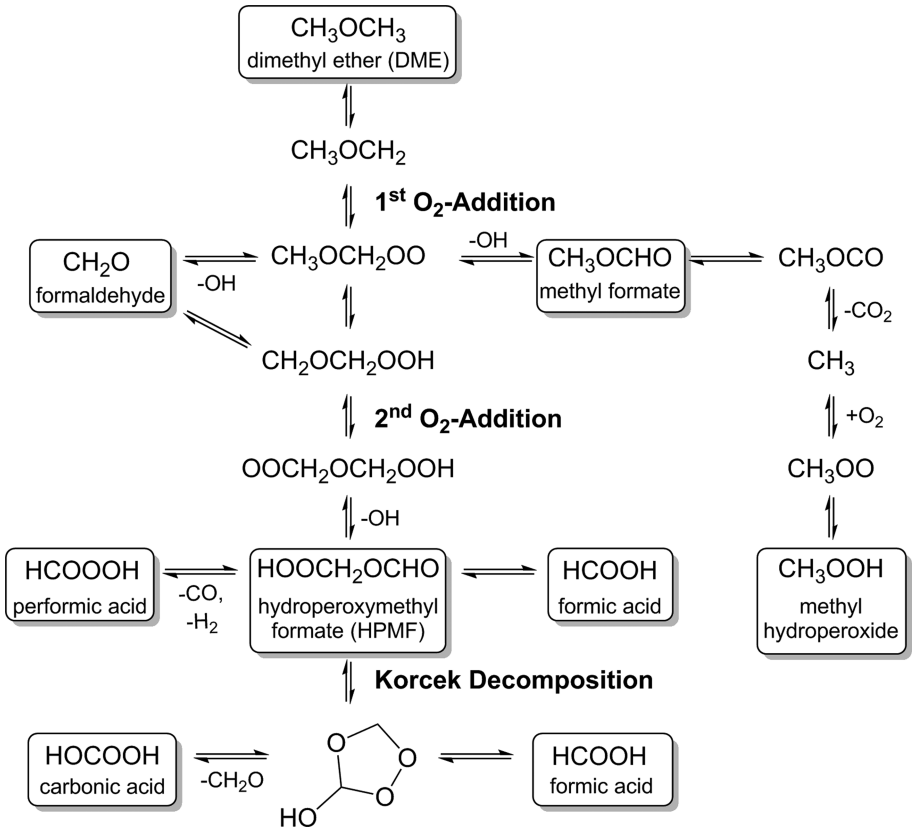

Figure 2. Schematic of the dimethyl ether oxidation steps at low temperatures. Species that are discussed in the main text are framed and shown with their respective name.

A pressure reduction from near-atmospheric pressure (933 mbar, 700 Torr) in the reactor to $\sim 10^{-4}$ mbar in the first pumping stage leads to the formation of a molecular beam in which further interactions between the molecules are prevented. This "freezing" of the chemistry in the molecular beam allows for the detection of highly reactive species. The central part of the molecular beam enters through a skimmer, the ionization region where it is crossed with the synchrotron-generated VUV photon beam (10^{14} photons/s). The tunability and resolution $[E/\Delta E(\text{fwhm}) \approx 250-400]$ of the photons' energy in the chemically interesting region from 7.4 to 30 eV allow for isomer specificity and near threshold ionization, i.e., reduced fragmentation.[20] The instrument's mass resolution of $m/\Delta m \approx 3500$ enables a detailed analysis of a complex mixture of oxygenates and hydrocarbons. Further details of the JSR system and the MBMS instrument can be found elsewhere.[6,21]

The reactor was operated at 23 different temperatures covering the low- and intermediate-temperature oxidation range of DME between 460 and 900 K. The temperatures were measured with a K-type thermocouple near the sampling position and, as will be discussed later, needed therefore to be corrected to account for a probe effect. The pressure in the JSR was kept constant at 933 mbar (700 Torr). Gas flows of DME, oxygen, and argon, which were controlled by calibrated mass flow controllers, were adjusted with changing temperatures to achieve a nominal residence time of τ = 4000 ms and a stoichiometry of ϕ = 0.35 while keeping an argon dilution of 78%. To derive the most reliable mole fraction profiles of the mixture's molecular components, the temperature-dependent mass spectra were recorded using photon energies of 10.2, 10.5, 11, 11.5, 14.35, and 16.65 eV. Figure 2 provides a general schematic diagram of DME's oxidation steps in the low-temperature regime. Species whose (quantified) temperature profiles are discussed below are framed and labeled with their respective names. For a more detailed description of the reactions the reader is referred to ref 6.

2.2. Data Evaluation. Mole fraction profiles were derived as a function of the mass-to-charge ratio (m/z) and temperature according to a procedure similar to the one commonly used for complementary flame-sampling mass-spectrometric studies,[22,23] which has been demonstrated to provide reliable quantitative data. Only the key points will be given in the next paragraphs.

The integrated ion signal S of a species i at a specific m/z ratio and an energy E is linked to its mole fraction x_i by the following relation:

$$S_i(E) = x_i \cdot \varphi \cdot \text{SW} \cdot D(M_i) \cdot c \cdot \text{FKT}(T) \cdot \sigma_i(E) \quad (1)$$

Here, φ is the number of photons, SW the number of sweeps, $D(M_i)$ the mass discrimination factor of species i, and c an instrument factor. FKT describes a temperature-dependent sampling function, and $\sigma_i(E)$ is the molecule-specific and energy-dependent photoionization cross section.

The determination of the mole fractions of the main species (DME, O_2, Ar, H_2O, CO, CO_2) is based on the mass spectra recorded at 14.35 and 16.65 eV while considering the element balance of C and H atoms. In this approach H_2 was not included because of its small signal in the mass spectra. Calibration factors for main species were calculated based on the flow conditions at the lowest reactor temperature for O_2 and DME (where no oxidation reactions occur) and at the highest reactor temperature for H_2O, CO, and CO_2 (where a

DOI: 10.1021/acs.jpca.6b06634
J. Phys. Chem. A 2016, 120, 7890−7901

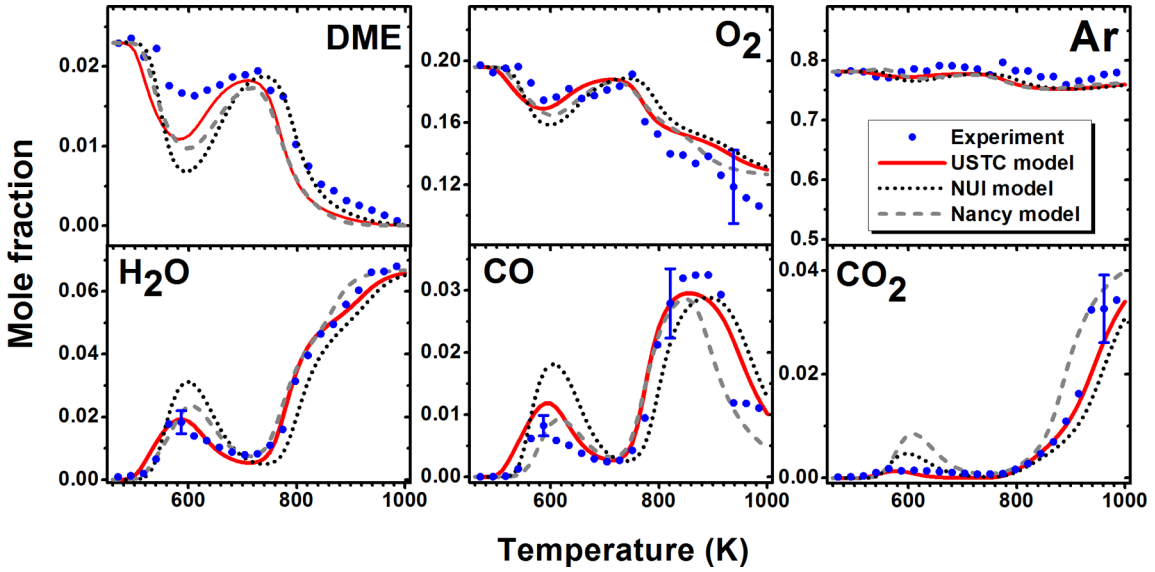

Figure 3. Experimental and simulated mole fraction profiles as a function of temperature of the main species (DME, O_2, Ar, H_2O, CO, CO_2) during the low- and intermediate-temperature oxidation of dimethyl ether. The experimental uncertainties are shown as error bars for some selected temperatures.

complete conversion of DME is observed). Subsequently, the argon mole fraction profile was calculated as the balance between the sum of all major species and unity.

The known argon mole fraction then allows for the determination of c·FKT(T) when mass discrimination factors (which were determined using standard calibration gases) and the photon flux (which was measured with a calibrated photodiode) are known. Subsequently, eq 1 is applied to calculate the mole fraction profile of the intermediate species employing an experimentally or theoretically determined PICS.

To first add confidence to our data evaluation procedure, we compared our experimentally obtained main species profiles with simulated concentration profiles using the three widely accepted DME mechanisms from ref 19 (USTC mech), ref 18 (NUI mech), and ref 5 (Nancy mech). The calculations were performed using the perfectly stirred reactor model within CHEMKIN-PRO.[24] The experimental and predicted mole fractions of DME, O_2, Ar, H_2O, CO, and CO_2 as a function of temperature are depicted in Figure 3. As can be seen, the mole fraction profiles reflect well the characteristic features of the low- and intermediate-temperature regime and within the expected uncertainties (±20%; see below) the experimental and modeled results are in acceptable agreement. This fact demonstrates the general reliability of our experimental data and of the data evaluation procedure.

All three mechanisms overpredict the consumption of DME in the low-temperature regime, and already for the major species unexpected large discrepancies exist between the model calculations (see Figure 3). For example, the USTC mech seems to be more reactive in the low-temperature regime than the other two mechanisms, and the models all predict different levels of DME conversion in the low-temperature regime near 600 K.

In order to achieve the general level of agreement between experiment and model predictions, the experimental data were shifted toward higher temperatures to match the characteristic peaks in the DME and CO profiles. An increasing heat flux to the cone with increasing temperatures was assumed. This approach results in a linearly increasing temperature shift of 10 K at the lowest and 85 K at the highest measured temperature, which seems reasonable considering the location of the thermocouple on the sampling probe (see Figure 1). The fact that the sampling probe is likely to serve as a heat sink is a known problem from the complementary flame-sampling experiments.[25] As a result of the probe heat-sink, the temperature measured by the thermocouple is expected to be lower than the actual temperature in the reactor. An actual measurement of this effect is currently not feasible, but the uncertainty of the corrected temperature was determined to be less than ±2.5%. A change in the reactor temperature also changes the residence time within the reactor because the inlet gas flow rates were fixed. The targeted residence time at each temperature condition was 4 s; however, the measured temperature is lower than the actual reactor temperature, so residence times are also lower than the targeted value. This fact results in residence times ranging from 3.9 to 3.2 s which were appropriately considered in the model calculations.

A detailed discussion of the associated error bars of the mole fractions can be found in ref 25. Uncertainties of ±20% for major species are expected. The accuracy of the absolute mole fractions for the intermediates depends mainly on the quality of the available photoionization cross sections. The uncertainty is generally on the order of a factor of 2 for intermediates with known PICS and can be as large as a factor of 4 when unknown PICS are used. Measured absolute cross sections are available for a variety of species[14] but are typically not available for highly reactive, short-lived species like they are present in the low-temperature oxidation regime. Unknown photoionization cross sections are sometimes estimated (for example, based on cross sections for similar species or using group additivity rules),[15,16] but the accuracy of these estimates and consequently the accuracy of the mole fractions might not be good enough to constrain the mechanisms as wanted. In the following section we will therefore discuss the potential of theory in providing scientifically based, reliable photoionization cross sections when experimentally not available and/or hard to obtain.

DOI: 10.1021/acs.jpca.6b06634
J. Phys. Chem. A 2016, 120, 7890−7901

3. THEORETICAL PHOTOIONIZATION CROSS SECTIONS

3.1. Methods. We considered two theoretical approaches for calculating absolute photoionization cross sections. In the first approach, the Franck−Condon overlap envelope, S, was included and σ was approximated

$$\sigma(E) = S(E)\cdot D(E) \quad (2)$$

The transition moment D was calculated using single channel frozen-core Hartree−Fock (FCHF) theory[26,27] and the ePolyScat codes of Lucchese et al.,[17] which have been used elsewhere[28−30] to calculate photoionization cross sections for a variety of systems. In the FCHF calculations, the geometries of the neutral species were optimized using M06-2X/cc-pVTZ, and their orbital energies were calculated using restricted HF/aug-cc-pVTZ. The value of D reported is the result of averaging the length and velocity gauges. Other than the orbital occupancy after ionization, no information about the cation is required to calculate D with this approach.

The Franck−Condon overlap envelope S was calculated using (rectilinear) normal modes and the usual separable-mode harmonic oscillator assumptions (calculated here at 0 K using Gaussian 09 and the M06-2X/cc-pVTZ level of theory). Franck−Condon transitions were summed and normalized such that S increased from 0 to 1 with increasing E. Because of the low rotational and vibrational temperature in the molecular beam, the use of overlaps calculated at 0 K is not likely a significant source of error.

In a second simpler approach, S was not calculated. Instead, eq 2 was applied where S was expected to be close to unity and therefore where

$$\sigma(E) \approx D(E) \quad (3)$$

If a clear "plateau" in the PICS can be identified and unambiguously associated with $S \approx 1$, then eq 3 may be expected to be just as reliable as eq 2. Equation 3 has the advantage that it can be applied for cases where S is difficult to calculate, as is the case for two species of interest in the present study: HPMF and CH_3OOH.

Lucchese and co-workers recently discussed cases where this single channel FCHF approach is not expected to be quantitative.[28] Specifically, the theoretical results were compared with measured PICS for several alkynes, and the authors characterized problems for systems with nearly degenerate occupied orbitals. We note that even for those cases where the single channel FCHF method was criticized, its error was found to be less than a factor of 2.

Similar maximum errors were reported in a recent study by Krylov and co-workers,[31] who tested their Dyson-orbital-based approach against measured photoionization spectra for several species. Their predicted results were compared with experimental cross sections for 15 atomic and molecular species, including five unsaturated hydrocarbons and three oxygenated species.

A similar validation study of eqs 2 and 3 has been performed as part of the present study for a test set of known PICS for 15 molecular and radical species. For nine of the test cases, S could be reliably calculated and eq 2 was applied. For the other species (which feature large amplitude torsions), the present method for calculating S is not expected to be accurate. The use of curvilinear coordinates (as used in ref 31 and elsewhere; e.g., see refs 32 and 33) may improve the accuracy of S for some of these species but was not considered here. Instead, eq 3 was applied and validated for all 15 species in the test set.

The results of the validation study are summarized next in section 3.2 and are presented in detail in the Supporting Information. In addition to difficulties associated with poor Franck−Condon overlaps, the application of the present theoretical approaches may be complicated by the presence of excited electronic states and fragmentation of the cation. In our validation study and applications, we attempted to minimize interference from these latter two effects by restricting attention to photon energies within ∼1 eV of the photoionization threshold. Examples of complications caused by poor Franck−Condon overlaps, fragmentation, and low-lying electronically excited states of the cation are discussed below for HPMF, CH_3OOH, and the CH_2O_3 isomers carbonic and performic acid.

3.2. Validation of the Theoretical Cross Sections. The FCHF method was tested against known experimental absolute photoionization profiles for 15 species: CH_3,[34−36] CH_4,[37−39] C_2H_2,[40−42] C_2H_4,[40,43,44] CH_2O,[45,46] HO_2,[45] formic acid [HC(O)OH],[47] propyne (CH_3CCH),[42,47] allene (CH_2CCH_2),[48−50] CH_3OH,[47] CH_3CHO,[49] DME,[49] $CH_3C(O)CH_3$,[47] CH_3OCHO,[51] and H_2O_2.[45] Detailed comparisons of eqs 2 and 3 with the experimental results for these 15 species are given in Supporting Information (Figures S2−S16), where the comparisons were used to assign a 2σ error bar of a factor of 2 to the theoretical cross sections.

A brief summary of the results of the validation study is reported here, with comparisons for three systems shown in Figure 4. In favorable cases where S is reliably computed and eq 2 is applied, the shapes and magnitudes of the calculated profiles can be very accurate, as shown in Figure 4a for CH_2O. Scaling the result of eq 2 for this system by 1.47 results in quantitative agreement with the measured profile, and as the scaling factor is independent of energy, it may be unambiguously assigned as the error in the calculated cross section. Furthermore, $S \approx 1$ just 0.3 eV above threshold, and the plateau region that follows at higher energies is free from electronically excited states and fragmentation. The use of the approximation to eq 2 in eq 3 therefore does not introduce any additional uncertainty for this system.

For more complex systems, such as CH_3CHO shown in Figure 4b, S cannot be reliably calculated using the simple approach described above. Nonetheless, the clear plateau region in the measured cross section at photon energies greater than 0.3 eV above threshold allows for the straightforward application of eq 3. The error in the calculated cross section can again be quantified by scaling the theoretical result to match the plateau region of the measured profile. The error for this system is just 15%. Again, there is no apparent contribution from excited electronic states or fragmentation over the first ∼1.25 eV of this spectrum.

For yet even more complex systems, such as DME shown in Figure 4c, the Franck−Condon overlap envelope could not be reliably calculated and is evidently broader than a few tenths of an eV, which leads to the absence of clear plateau region within the first few eV above threshold. The present theoretical approach is less reliable for these cases, but we nonetheless assume that S approaches unity after ∼1 eV. This assumption leads to a quantified error of 25% in the calculated cross section for DME, which is consistent with the systems compared in Figure 4a and Figure 4b and with the larger test set included in the Supporting Information. While the absence of a clear

DOI: 10.1021/acs.jpca.6b06634
J. Phys. Chem. A 2016, 120, 7890−7901

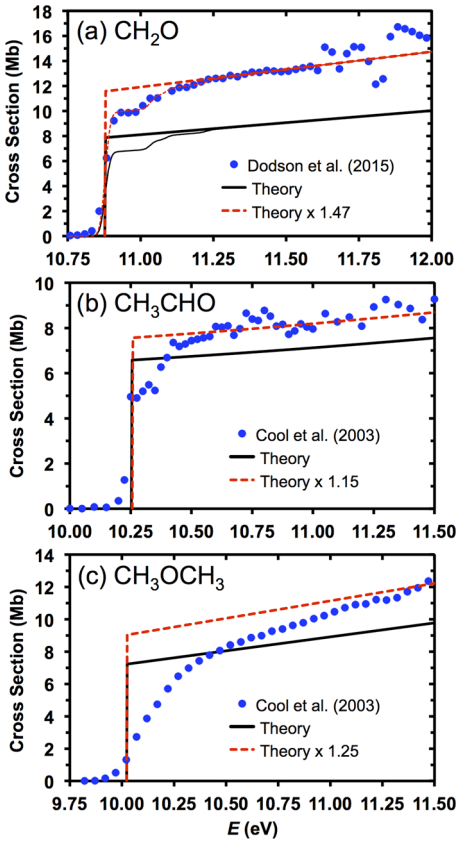

Figure 4. Theoretical (black lines) and scaled theoretical (red lines) cross sections for (a) CH_2O, (b) CH_3CHO, and (c) DME. The thick lines are the results of eq 3, and the thin lines in (a) are the results of eq 2. Experimental cross sections (blue circles, CH_2O, ref 45; CH_3CHO, ref 49; DME, ref 49) are also shown.

plateau region introduces additional ambiguities in the present approach, these errors are likely smaller than the absolute error of a factor of 2 assigned to the theoretical approach.

Although not encountered for the examples given in Figure 4, the application of the present theoretical approach may be further complicated by the presence of excited electronic states and fragmentation of the cation. Excited electronic states are readily treated using the present approach. The additional threshold energies and transition dipole moments associated with excited electronic states of the cation may be calculated, and the total cross section could be calculated using eqs 2 and 3 and summing over the contributions from each electronic state. Low-lying excited electronic states of the peroxide cations are of particular relevance in the present study. As shown in the Supporting Information, the cation of H_2O_2 features an excited electronic state just 0.35 eV above its first ionization threshold. We therefore considered excited electronic states for the two peroxides (CH_3OOH and HPMF) quantified below.

The theoretical results obtained here correspond to the total photoionization cross section and include any fragmentation channels. Fragmentation channels would necessarily appear experimentally at different m/z, and even for moderately sized systems, fragmentation can occur close to the ionization threshold. Appearance energies may be readily calculated, and in principle, branching to the various fragmentation channels could be quantified. Such branching calculations are not attempted here, as they would be computationally demanding and would likely feature significant uncertainty. Fragmentation significantly complicates the quantification of the species concentration of HPMF, as discussed in detail below.

4. RESULTS AND DISCUSSION

In order to validate the low-temperature part of the DME combustion chemistry mechanisms[5,18,19] and to identify opportunities for improvements, the quantification of the combustion reactants, intermediates, and products is crucial. The experimental mole fraction profiles of the main species (H_2O, CO, O_2, Ar, CO_2, and DME) as a function of the reactor temperature were shown in Figure 3 and discussed together with the model predictions in the experimental section 2.2 as part of the data evaluation procedures. In summary, an overprediction was observed for the DME consumption in the low-temperature regime in the models' predictions.

The mole fraction profiles of CH_4, C_2H_2, C_2H_4, C_2H_6, CH_2O, and CH_3OH, which were determined using eq 1 in combination with literature-known PICS,[37,46,47,52] are shown together with the corresponding model predictions in the Supporting Information (Figure S1). In the following, we discuss the mole fraction profiles of the elusive intermediates H_2O_2, CH_3OCHO, and CH_2O_2, which identify inconsistencies between the mechanisms with regard to the general description of the low-temperature oxidation chemistry of DME. Especially the discussion about the CH_2O_2 chemistry highlights the need to probe the HPMF chemistry accurately. Therefore, we provide the most reliable mole fraction profiles possible for CH_3OOH and HPMF using the theoretically calculated PICS, as described in the previous section. In the last part, we provide further validation targets for the HPMF chemistry in the form of the temperature profiles for the isomeric CH_2O_3 intermediates, which were identified as the HPMF decomposition products performic and carbonic acid [HC(O)OOH and HOC(O)OH] in ref 6. This section of the paper also includes a discussion of the limitations of our approach to determine PICS with respect to the separation and quantification of isomeric species.

4.1. Mole Fraction Profiles of Intermediates with Literature Available Photoionization Cross Sections: H_2O_2, CH_2O_2, and CH_3OCHO. Figure 3 has revealed that all three DME mechanisms (USTC,[19] NUI,[18] and Nancy[5]) considered here differ already significantly in their predictions for the main species profiles. In the following discussion only a few comparisons between the mechanisms' different description of the detailed chemistry are provided and instead we refer the reader to the papers, in which the mechanisms have been described, for the origins of the different predictions.[5,18,19] In order to suggest targeted refinements to the mechanisms, it is crucial to further constrain them with reliable quantitative intermediate species profiles. As mentioned earlier, the low-temperature oxidation of DME involves many partially oxidized and elusive intermediate species. Their simultaneous detection and quantification are made possible here by employing molecular-beam mass spectrometry in combination with VUV single-photon ionization. Figure 5 shows the experimental concentration profiles of (a) H_2O_2 (hydrogen peroxide), (b) CH_3OCHO (methyl formate), and (c) CH_2O_2 (formic acid), which are well-known intermediates during the oxidation of DME. However, quantitative reference data of these species are sparse.[53−57] The mole fraction profiles were derived with eq 1 by using published photoionization cross sections.[45,47,51] These new data shown here can serve as validation targets for present

DOI: 10.1021/acs.jpca.6b06634
J. Phys. Chem. A 2016, 120, 7890−7901

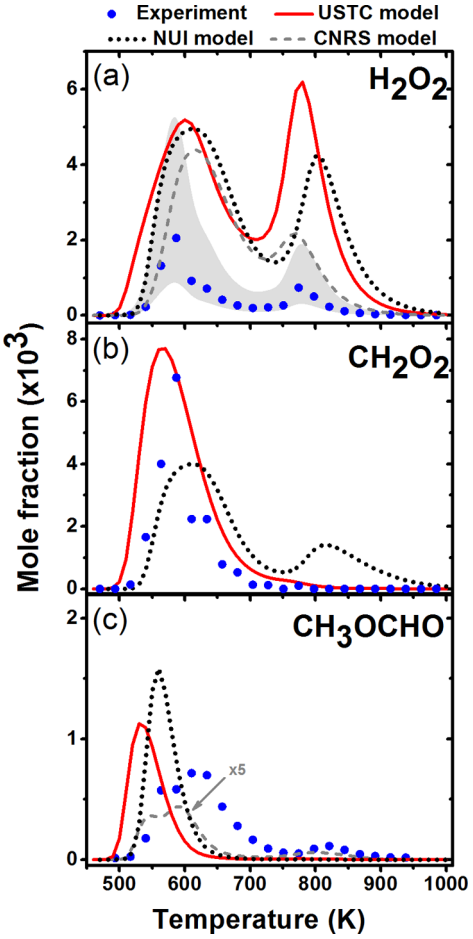

Figure 5. (a) Experimental and modeled mole fraction profiles of hydrogen peroxide, (b) formic acid, and (c) methyl formate. Exemplary error bars (gray shaded area) are added.

and future mechanisms, and consequently, we compared our experimental data with modeling results using the three mechanisms mentioned above.

It is obvious from Figure 5 that the USTC mech generally predicts a higher reactivity shifted toward the lower temperature range when compared to the NUI and the Nancy mechanisms; the onset of the low-temperature combustion is outside the experimental error limits as described above. Similar trends are visible also in the main species profiles shown in Figure 3 and the intermediate profiles shown in Figure S1. Compared to the USTC and NUI mechanisms, the Nancy mech succeeds in predicting the species' peak positions for most of the intermediates in the low-temperature regime better than the other two models.

Specifically for H_2O_2 [see Figure 5a], all three models predict larger concentrations in the low-temperature regime than experimentally observed, but this discrepancy in the peak concentrations is expected to be still within the experimental uncertainty, which is depicted as a gray shaded area. The Nancy mech predicts the temperature of the maximum concentration to be at a higher temperature than experimentally observed, while NUI and USTC mechanisms show a better agreement between theoretical and experimental data with regard to the mole fraction peak position in the low-temperature regime. Both the NUI and Nancy mechanisms reproduce well the beginning of the H_2O_2 formation at the low temperatures near 530 K. As mentioned above, the USTC mech predicts a slightly earlier formation of H_2O_2 around 500 K, with this deviation being outside the experimental error limits.

A second peak in the H_2O_2 concentration appears at temperatures above 700 K. Its concentration was determined experimentally to be 36% lower than in the low-temperature regime. This trend in the relative concentrations is also observed in the modeling results based on the latest Nancy and NUI mechanism, predicting 51% and 15% decrease in relative peak concentration, respectively. In contrast, the USTC mech predicts a slightly higher (19%) concentration of the second peak. Overall, the peak concentrations of H_2O_2 in the intermediate temperature regime based on the three different mechanisms differ by a factor of 3 and only the Nancy model results are sufficiently close to the experimentally obtained mole fractions (considering the experimental uncertainties as illustrated by the gray shaded area).

Reasonable agreement between modeled and experimental data is also found for the mole fraction profiles of methyl formate (CH_3OCHO) computed with the USTC and NUI mechanisms, whereas the Nancy mech underpredicts the experimental data by a factor of 8 [see Figure 5b]. A similar level of underprediction was also observed in the fuel-lean case studied by Rodriguez et al.[5] using the Nancy mechanism. This deviation is outside the experimental error limits. Overall the experimental profile spans a broader temperature range than predicted by all three models. Note that 1,3-dioxetane was identified as an isomer on the same mass.[6] This intermediate species was not considered in the data evaluation due to its very low concentration, and the resulting error is considered to be within 1% on the methyl formate concentration based on the photoionization efficiency (PIE) curve reported in ref 6.

Interestingly, the Nancy mech is capable of predicting the double-peak feature in the low-temperature regime measured in the experiment for CH_3OCHO. In addition, a smaller second peak in the intermediate-temperature range can be seen at 820 K, which was also observed in the study of Rodriguez et al.[5] This peak is currently only predicted by the Nancy mechanism.

Reasonable agreement between experimental and modeled mole fractions can be found for formic acid (CH_2O_2); see Figure 5c. Note that formic acid is not included in the Nancy mechanism. For the USTC mech, a higher reactivity can be observed, while the NUI mech predicts the onset at low temperatures very well. In the latter mechanism, formic acid is a direct oxidation product of DME via the keto-hydroperoxide HPMF forming OCH_2OCHO as an intermediate. The fact that the description of the decomposition of this radical intermediate is different in the two mechanisms might explain their different predictions. Specifically, in the USTC mech, OCH_2OCHO decomposes directly to form CH_2O_2 and HCO, while in the NUI mech, the formation of CH_2O_2 is described in sequential steps via $HOCH_2OCO$ and $HOCH_2O$. In the Nancy mech, OCH_2OCHO decomposes entirely to form CH_2O and the OCHO radical, thus not forming any formic acid.

A second peak in the intermediate-temperature regime, as predicted from the NUI mechanism, was not observed in the experiment. As pointed out by Wang et al.,[19] this peak results from a large reaction rate of the OH addition to CH_2O forming $HOCH_2O$, which serves as precursor for CH_2O_2.

The above discussion about the differences between the mechanisms and their ability to reasonably predict the experimental results highlights the importance to further constrain mechanistic developments. Especially, new knowl-

DOI: 10.1021/acs.jpca.6b06634
J. Phys. Chem. A 2016, 120, 7890−7901

edge about concentrations of highly elusive species, like the HPMF, that have been historically hard to detect should be key to refining the mechanism describing the low-temperature chemistry.

4.2. Mole Fraction Profiles of Intermediates with Calculated Photoionization Cross Sections: CH_3OOH and HPMF. The quantification of CH_3OOH and HPMF is more challenging because their photoionization cross sections have not been measured. The theoretical approach described in section 3 to predict photoionization cross sections was first applied for the CH_3OOH system, which is expected to be much simpler to handle than the structurally more complex keto-hydroperoxide. We then used this new approach to provide reliable mole fraction data for HPMF.

Figure 6a shows the theoretically obtained photoionization cross section of CH_3OOH together with the JSR-sampled PIE

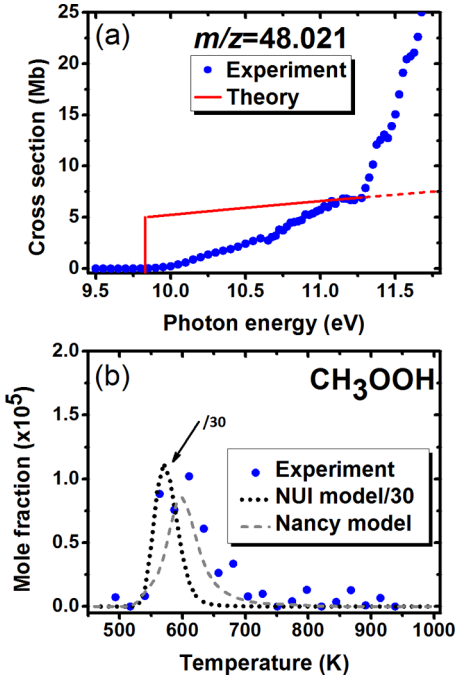

Figure 6. (a) Calculated photoionization cross section (thick red line) of CH_3OOH and scaled experimental PIE curve of m/z = 48.021 u. (b) Obtained experimental and modeled temperature-dependent mole fraction profiles of CH_3OOH.

curve of m/z = 48.021 u. On the basis of the discussion in section 3, the flat part between 11.05 and 11.3 eV was scaled to a value of 6.88 Mb, which is the theoretically calculated photoionization cross section at 1.3 eV above the ionization energy (calcd IE = 9.83 eV).[6] The increase in the photoionization efficiency at ~11.25 eV is not attributed to ground-state photoionization, as discussed below. By use of the experimentally observed PIE curve along with the absolute value from theory, a cross section of 1.15 Mb at 10.2 eV was derived.

The resulting experimental mole fraction profile of CH_3OOH using the theoretically determined cross section is shown in Figure 6b. The obtained peak value of 1.1×10^{-5} seems to be reasonable, and the profile shape, position, and magnitude as predicted with the Nancy mech are in excellent agreement with the experimental results. However, modeling results using the Nancy and NUI mechanisms reveal a huge discrepancy in the peak concentrations, while CH_3OOH is not even included in the USTC mechanism. The most important reaction, which is responsible for the formation of CH_3OOH in both the Nancy and NUI mechanisms, is $CH_3O_2 + OOH \rightleftarrows CH_3OOH + O_2$. Interestingly, the rate constants are similar but the overall rate of production differs significantly. This observation was traced back to differences in the predicted concentrations of the CH_3O_2 and OOH radicals, which are about one order of magnitude.

As discussed above, the general usefulness of the present approach to calculate required cross sections is limited by several factors, particularly for systems with extended Franck–Condon envelopes, low-lying excited electronic states of the cation, and fragmentation of the cation. For CH_3OOH the latter was not considered because its fragmentation is known not to start below 11.5 eV.[58] The signal increase above 11.3 eV [visible in Figure 6a] falls together with the lowest-lying excited electronic state of the cation for CH_3OOH, which was calculated to be 1.6 eV above the ground electronic state of the cation. This increase could also be caused by the isomeric methanediol (calcd IE = 11.10 eV),[6] but its presence in the low-temperature oxidation regime of DME is unknown. Both facts do not influence our determination of the necessary cross section values in the chosen energy range.

As for the HPMF, the quantification procedure becomes more challenging because of significant fragmentation close to the threshold.[6] As pointed out before, the theoretical results obtained here correspond to the total photoionization cross section and include fragmentation channels. As a consequence, an accurate determination of the cross section of any given species requires the knowledge of its energy-dependent fragmentation pattern and thus the complete understanding of the mass spectra.

HPMF can undergo several fragmentations: a CO loss from the formate group, an H atom loss, and the loss of the HOO group, appearing above 10.07, 10.6, and 10.92 eV respectively.[6] All of these appearance energies are within the first 1.0–1.5 eV above the ionization energy of HPMF (~10.0 eV), and resulting fragmentation pattern therefore has to be considered in the determination of HPMF's photoionization cross section.

The total ion signal of HPMF, which was obtained by adding together the individual contributions from the known fragment signals, is depicted in Figure 7a together with the measured PIE curve of m/z = 92.021 u. Note that the main contribution to the total ion signal stems from the fragment on m/z = 64.016 u (CH_4O_3), while the signal of m/z = 92.021 u is multiplied by a factor of 50 for better visualization. At energies 1.4–1.6 eV above the threshold no additional fragments are observed, thus the signal stays flat. This part of the curve was fitted to a value of 6.56 Mb, the theoretically calculated photoionization cross section 1.5 eV above the IE, leading to a partial photoionization cross section of 0.017 Mb at 10.2 eV for HPMF's parent ion. The obtained value seems fairly small but reasonable considering the favored dissociation of the HPMF cation onto m/z = 64.016 u.

Using the obtained value of 0.017 Mb at 10.2 eV results in a peak concentration of 9.1×10^{-4}. The entire experimental mole fraction profile is shown together with the corresponding modeled profiles in Figure 7b. Considering the source of our cross section value, i.e., not estimated but calculated based on a theoretical approach, this is the most reliable determination of the mole fraction profile currently possible. Its agreement with the peak mole fraction simulated with the USTC mech is

DOI: 10.1021/acs.jpca.6b06634
J. Phys. Chem. A 2016, 120, 7890–7901

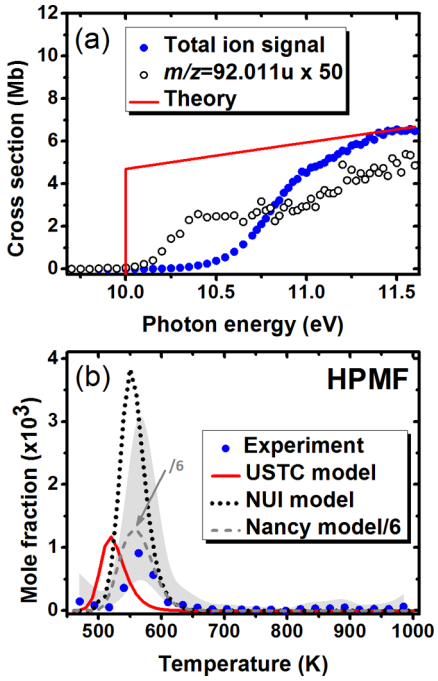

Figure 7. (a) Total ion signal of HPMF including the contributions of the parent ion and its fragments and the measured PIE curve of m/z = 92.021 multiplied by 50. Theoretically calculated total photoionization cross sections are shown as thick red line. (b) Experimental and simulated temperature-dependent mole fraction profile of HPMF. Exemplary error bars (gray shaded area) are added.

remarkable. However, a temperature shift to lower temperatures is observed for the model predictions. The NUI and Nancy mechanisms overpredict the concentration of the keto-hydroperoxide, and their results are outside of the provided experimental error bars.

The keto-hydroperoxide HPMF is a direct oxidation product of DME oxidation, and its concentration is therefore extremely useful for mechanism validation. According to the model calculations, the mole fraction profile of HPMF results from the formation reaction via $OOCH_2OCH_2OOH \rightleftarrows HOOCH_2OCHO + OH$ and its dissociation via $HOOCH_2OCHO \rightleftarrows OCH_2OCHO + OH$. When the modeling results are analyzed, the following things were noticed: (a) The three models predict similar levels of the $OOCH_2OCH_2OOH$ peak concentration. (b) The same rate expressions are used for the above-mentioned formation reaction of HPMF in the USTC and Nancy mechanisms. The different rates of production of HPMF in the two model predictions are thus likely to be a consequence of the different thermodynamic data used in the mechanisms. (c) The NUI mech results in a similar rate of production for HPMF than the Nancy mechanism. However, the NUI mech includes faster rates for HPMF formation than the other two mechanisms; thus the similarity in the rate of production can again be traced back to the differences in the thermodynamic data. (d) With regard to the decomposition reaction of HPMF into $OCH_2OCHO + OH$, all mechanisms use similar rate expressions. The differences in the rate of consumption result from the different initial concentration of the HPMF and the thermodynamic data. Again, it is not the authors' intention to judge the quality of the models' description of the detailed chemistry, and it is out of the scope of the present paper to consolidate the modeling efforts. However, the discussion clearly highlights the need of reliable reference data, as provided here for the first time, and the reported mole fraction profiles for CH_3OOH and HPMF should be used as validation targets for future model developments.

As discussed in ref 6, the model's description of the HPMF chemistry can be more complete when including further decomposition products, like the previously identified performic and carbonic acid. Their temperature profiles are discussed next, also describing the limitations of our theoretical approach to obtain photoionization cross sections when isomeric species are present.

4.3. Limitations of the Theoretical Approach: Temperature Profiles of CH_2O_3 Intermediates. The separation of combustion relevant isomers and their quantification via photoionization molecular beam mass spectrometry has been demonstrated many times in flame-sampling experiments.[16,25] This quantification procedure requires knowing the photoionization cross sections of each isomer. The applicability of the previously presented method to determine photoionization cross sections is limited if two or more isomers contribute to the PIE curve within the first 1.5 eV over the lowest threshold. Performic acid and carbonic acid, both identified as intermediates in the low-temperature oxidation regime of DME,[6] represent such a case.

At photon energies 1.5 eV above the threshold of performic acid both species contribute to the measured PIE curve on m/z = 62.000 u (calcd IEs: performic acid 10.87 eV; carbonic acid 11.29 eV). As a consequence, the measured PIE curve does not contain a part in which overlaps can be neglected; this makes the determination of these species' cross sections hardly possible with this simple approach, and experimental mole fraction profiles cannot be obtained here.

However, the qualitative temperature profile of performic acid could be extracted from the measured signal at 11 eV (below the ionization energy of carbonic acid). It is plotted together with the calculated profile from the NUI mech in Figure 8. In this case, the model underpredicts DME's reactivity

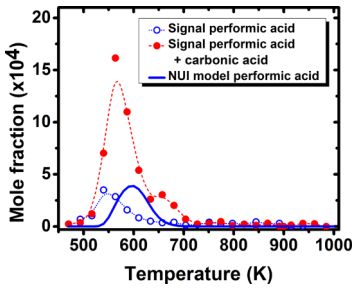

Figure 8. Experimental temperature profiles of performic acid extracted from the measured signal at 11 eV and the respective modeling results from the NUI mechanism (thick line). The signal at 11.5 eV includes the contribution of carbonic acid.

and the profile is shifted to higher temperatures compared to the experimental data. Reactions of performic acid are not included in the Nancy and USTC mechanisms.

Without a known mole fraction profile of performic acid, the extraction of a pure temperature profile of carbonic acid is not possible. Nonetheless, the combined temperature profile of performic and carbonic acid can be extracted from the mass spectra recorded at 11.5 eV. As can be seen from Figure 8, it holds some interesting features. Specifically, the peak of the combined signal is shifted about 20 K toward higher

DOI: 10.1021/acs.jpca.6b06634
J. Phys. Chem. A 2016, 120, 7890−7901

temperatures, indicating that the carbonic acid reaches its peak concentration at slightly higher temperatures than performic acid. Additionally, a second peak appears at 657 K, which is not observed in the profile of performic acid. This peak indicates that two different formation channels of carbonic acid exist. Carbonic acid, which potentially is an indication for the so-called Korcek decomposition mechanism of the HPMF,[6] is absent from the three mechanisms applied here.

5. SUMMARY AND CONCLUSIONS

In this paper we have provided quantitative information about the hydroperoxymethyl formate (HPMF, $HOOCH_2OCHO$) and other oxygenated intermediate species (CH_2O, CH_3OH, H_2O_2, CH_2O_2, CH_3OOH, CH_3OCHO) in the low-temperature regime of dimethyl ether (DME) oxidation. The key to the quantification of the elusive HPMF and CH_3OOH was the combination of experimental and theoretical work. The experiment, which used a jet-stirred reactor coupled to a mass spectrometer with VUV single-photon ionization, provides temperature-dependent mass spectra recorded at different photon energies and photoionization efficiency curves including molecule-specific fragmentation patterns. The key theoretical aspect of this work was the validation and application of a theoretical approach that provides calculated photoionization cross sections close to the ionization threshold even if Franck−Condon overlaps cannot be calculated easily. The use of this theoretically determined photoionization cross section provides a scientifically based mole fraction profile which is therefore more reliable than concentrations obtained with estimated PICS.

The applied theoretical approach requires several experimentally determined molecule-specific information that includes a known experimental PIE curve and a detailed knowledge of the species' energy-dependent fragmentation patterns. Considering the complex mixture in combustion environments, low mass fragments might sometimes be hard to identify and quantify. As a consequence, a fundamental and complete understanding of the recorded mass spectra is required. The method used here is relatively simple, as we have restricted attention to only the first 1.5 eV above threshold to minimize the effects of excited electronic states and fragmentation of the cation. Quantitative information can be difficult to extract with this approach when the species of interest feature broad Franck−Condon overlaps, significant fragmentation, and two or more overlapping isomers. Despite these limitations, the method is expected to often be accurate to better than a factor of 2, as quantified by comparisons with measured cross sections for 15 species.

The experimentally determined mole fraction profiles were compared with model predictions using rigorously tested DME oxidation mechanisms that are currently available.[5,18,19] It is apparent that the model predictions and the underlying chemistry vary significantly, thus highlighting the need to further constrain mechanisms in the future. On the basis of the newly reported mole fraction profiles alone, it is not possible to identify specific rates for improving the description of the DME low-temperature oxidation in the mechanisms. However, the quantification of the hydroperoxymethyl formate HPMF, which is known to be an important intermediate for chain-branching in the low-temperature combustion of DME, provides guidance for the development of next-generation low-temperature oxidation mechanisms of DME.

■ ASSOCIATED CONTENT

Supporting Information

The Supporting Information is available free of charge on the ACS Publications website at DOI: 10.1021/acs.jpca.6b06634.

Additional mole fraction profiles and validation study of the theoretical photoionization cross sections (PDF)

■ AUTHOR INFORMATION

Corresponding Author

*Phone: +1-925-294-6272. E-mail: nhansen@sandia.gov.

Present Address

#K.M.: Physikalisch-Technische Bundesanstalt, Bundesallee 100, D-38116 Braunschweig, Germany.

Notes

The authors declare no competing financial interest.

■ ACKNOWLEDGMENTS

This material is based upon work supported by the U.S. Department of Energy (DOE), Office of Science, Office of Basic Energy Sciences. D.M.P.-V. is supported by the DOE Gas Phase Chemical Physics Program at Lawrence Berkeley National Laboratory, under Contract DEAC02-05CH11231. We thank Paul Fugazzi for technical assistance and Profs. Leone, Sarathy, and Kohse-Höinghaus for continuing support of this project, and Prof. Lucchese for providing his code. P.D. received funding from the European Research Council under the European Community's Seventh Framework Programme (FP7/2007-2013)/ERC Grant Agreement 291049-2G-CSafe. Z.W. and V.S.B.S. acknowledge competitive research funding given to the Clean Combustion Research Center from the King Abdullah University of Science and Technology. The Advanced Light Source is supported by the Director, Office of Science, Office of Basic Energy Sciences, of the U.S. DOE under Contract DEAC02-05CH11231. Sandia is a multimission laboratory operated by Sandia Corporation, a Lockheed Martin Company, for the National Nuclear Security Administration under Contract DE-AC04-94-AL85000.

■ REFERENCES

(1) Jacobs, T. J.; Assanis, D. N. The attainment of premixed compression ignition low-temperature combustion in a compression ignition direct injection engine. *Proc. Combust. Inst.* **2007**, *31* (2), 2913−2920.

(2) Arcoumanis, C.; Bae, C.; Crookes, R.; Kinoshita, E. The potential of dimethyl ether (DME) as an alternative fuel for compression-ignition engines: A review. *Fuel* **2008**, *87* (7), 1014−1030.

(3) Azizi, Z.; Rezaeimanesh, M.; Tohidian, T.; Rahimpour, M. R. Dimethyl ether: A review of technologies and production challenges. *Chem. Eng. Process.* **2014**, *82*, 150−172.

(4) Semelsberger, T. A.; Borup, R. L.; Greene, H. L. Dimethyl ether (DME) as an alternative fuel. *J. Power Sources* **2006**, *156* (2), 497−511.

(5) Rodriguez, A.; Frottier, O.; Herbinet, O.; Fournet, R.; Bounaceur, R.; Fittschen, C.; Battin-Leclerc, F. Experimental and modeling investigation of the low-temperature oxidation of dimethyl ether. *J. Phys. Chem. A* **2015**, *119* (28), 7905−7923.

(6) Moshammer, K.; Jasper, A. W.; Popolan-Vaida, D. M.; Lucassen, A.; Diévart, P.; Selim, H.; Eskola, A. J.; Taatjes, C. A.; Leone, S. R.; Sarathy, S. M.; et al. Detection and identification of the keto-hydroperoxide ($HOOCH_2OCHO$) and other intermediates during low-temperature oxidation of dimethyl ether. *J. Phys. Chem. A* **2015**, *119* (28), 7361−7374.

(7) Knox, J. H. A new mechanism for the low temperature oxidation of hydrocarbons in the gas phase. *Combust. Flame* **1965**, *9* (3), 297−310.

DOI: 10.1021/acs.jpca.6b06634
J. Phys. Chem. A 2016, 120, 7890−7901

(8) Benson, S. W. Effects of Resonance and Structure on the Thermochemistry of Organic Peroxy Radicals and the Kinetics of Combustion Reactions. *J. Am. Chem. Soc.* **1965**, *87* (5), 972−979.
(9) Miller, J. A.; Pilling, M. J.; Troe, J. Unravelling combustion mechanisms through a quantitative understanding of elementary reactions. *Proc. Combust. Inst.* **2005**, *30* (1), 43−88.
(10) Hansen, N.; Merchant, S. S.; Harper, M. R.; Green, W. H. The predictive capability of an automatically generated combustion chemistry mechanism: Chemical structures of premixed iso-butanol flames. *Combust. Flame* **2013**, *160* (11), 2343−2351.
(11) Battin-Leclerc, F.; Herbinet, O.; Glaude, P.-A.; Fournet, R.; Zhou, Z.; Deng, L.; Guo, H.; Xie, M.; Qi, F. Experimental confirmation of the low-temperature oxidation scheme of alkanes. *Angew. Chem., Int. Ed.* **2010**, *49* (18), 3169−3172.
(12) Battin-Leclerc, F.; Herbinet, O.; Glaude, P. A.; Fournet, R.; Zhou, Z. Y.; Deng, L. L.; Guo, H. J.; Xie, M. F.; Qi, F. New experimental evidences about the formation and consumption of ketohydroperoxides. *Proc. Combust. Inst.* **2011**, *33* (1), 325−331.
(13) Savee, J. D.; Papajak, E.; Rotavera, B.; Huang, H. F.; Eskola, A. J.; Welz, O.; Sheps, L.; Taatjes, C. A.; Zador, J.; Osborn, D. L. Direct observation and kinetics of a hydroperoxyalkyl radical (QOOH). *Science* **2015**, *347* (6222), 643−646.
(14) *Photonionization Cross Section Database*, version 1.0; National Synchrotron Radiation Laboratory: Hefei, China, 2011; http://flame.nsrl.ustc.edu.cn/en/database.htm.
(15) Hansen, N.; Cool, T. A.; Westmoreland, P. R.; Kohse-Höinghaus, K. Recent contributions of flame-sampling molecular-beam mass spectrometry to a fundamental understanding of combustion chemistry. *Prog. Energy Combust. Sci.* **2009**, *35* (2), 168−191.
(16) Qi, F. Combustion chemistry probed by synchrotron VUV photoionization mass spectrometry. *Proc. Combust. Inst.* **2013**, *34* (1), 33−63.
(17) Lucchese, R. R.; Sanna, N.; Natalense, A. P. P.; Gianturco, F. A. *ePolyScat*, version E3; Texas A&M University: College Station, TX.
(18) Burke, U.; Somers, K. P.; O'Toole, P.; Zinner, C. M.; Marquet, N.; Bourque, G.; Petersen, E. L.; Metcalfe, W. K.; Serinyel, Z.; Curran, H. J. An ignition delay and kinetic modeling study of methane, dimethyl ether, and their mixtures at high pressures. *Combust. Flame* **2015**, *162* (2), 315−330.
(19) Wang, Z.; Zhang, X.; Xing, L.; Zhang, L.; Herrmann, F.; Moshammer, K.; Qi, F.; Kohse-Höinghaus, K. Experimental and kinetic modeling study of the low- and intermediate-temperature oxidation of dimethyl ether. *Combust. Flame* **2015**, *162* (4), 1113−1125.
(20) Leone, S. R.; Ahmed, M.; Wilson, K. R. Chemical dynamics, molecular energetics, and kinetics at the synchrotron. *Phys. Chem. Chem. Phys.* **2010**, *12* (25), 6564−6578.
(21) Lucassen, A.; Park, S.; Hansen, N.; Sarathy, S. M. Combustion chemistry of alcohols: Experimental and modeled structure of a premixed 2-methylbutanol flame. *Proc. Combust. Inst.* **2015**, *35* (1), 813−820.
(22) Osswald, P.; Struckmeier, U.; Kasper, T.; Kohse-Höinghaus, K.; Wang, J.; Cool, T. A.; Hansen, N.; Westmoreland, P. R. Isomer-specific fuel destruction Ppthways in rich flames of methyl acetate and ethyl formate and consequences for the combustion chemistry of esters. *J. Phys. Chem. A* **2007**, *111* (19), 4093−4101.
(23) Schenk, M.; Leon, L.; Moshammer, K.; Oßwald, P.; Zeuch, T.; Seidel, L.; Mauss, F.; Kohse-Höinghaus, K. Detailed mass spectrometric and modeling study of isomeric butene flames. *Combust. Flame* **2013**, *160* (3), 487−503.
(24) *CHEMKIN-PRO*; Reaction Design: San Diego, CA, 2015.
(25) Egolfopoulos, F. N.; Hansen, N.; Ju, Y.; Kohse-Höinghaus, K.; Law, C. K.; Qi, F. Advances and challenges in experimental research of combustion chemistry in laminar flames. *Prog. Energy Combust. Sci.* **2014**, *43* (1), 36−67.
(26) Gianturco, F. A.; Lucchese, R. R.; Sanna, N. Calculation of low-energy elastic cross sections for electron-CF4 scattering. *J. Chem. Phys.* **1994**, *100* (9), 6464−6471.
(27) Natalense, A. P. P.; Lucchese, R. R. Cross section and asymmetry parameter calculation for sulfur 1s photoionization of SF6. *J. Chem. Phys.* **1999**, *111* (12), 5344−5348.
(28) Jacovella, U.; Holland, D. M. P.; Boyé-Péronne, S.; Gans, B.; de Oliveira, N.; Ito, K.; Joyeux, D.; Archer, L. E.; Lucchese, R. R.; Xu, H.; Pratt, S. T. A Near-Threshold Shape Resonance in the Valence-Shell Photoabsorption of Linear Alkynes. *J. Phys. Chem. A* **2015**, *119*, 12339.
(29) Jacovella, U.; Holland, D. M. P.; Boyé-Péronne, S.; Gans, B.; de Oliveira, N.; Joyeux, D.; Archer, L. E.; Lucchese, R. R.; Xu, H.; Pratt, S. T. High-resolution vacuum-ultraviolet photoabsorption spectra of 1-butyne and 2-butyne. *J. Chem. Phys.* **2015**, *143* (3), 034304.
(30) Gans, B.; Boye-Peronne, S.; Broquier, M.; Delsaut, M.; Douin, S.; Fellows, C. E.; Halvick, P.; Loison, J.-C.; Lucchese, R. R.; Gauyacq, D. Photolysis of methane revisited at 121.6 nm and at 118.2 nm: quantum yields of the primary products, measured by mass spectrometry. *Phys. Chem. Chem. Phys.* **2011**, *13* (18), 8140−8152.
(31) Gozem, S.; Gunina, A. O.; Ichino, T.; Osborn, D. L.; Stanton, J. F.; Krylov, A. I. Photoelectron Wave Function in Photoionization: Plane Wave or Coulomb Wave? *J. Phys. Chem. Lett.* **2015**, *6*, 4532−4540.
(32) Reimers, J. R. A practical method for the use of curvilinear coordinates in calculations of normal-mode-projected displacements and Duschinsky rotation matrices for large molecules. *J. Chem. Phys.* **2001**, *115* (20), 9103−9109.
(33) Vogelhuber, K. M.; Wren, S. W.; McCoy, A. B.; Ervin, K. M.; Lineberger, W. C. Photoelectron spectra of dihalomethyl anions: Testing the limits of normal mode analysis. *J. Chem. Phys.* **2011**, *134* (18), 184306.
(34) Gans, B.; Mendes, L. A. V.; Boyé-Péronne, S.; Douin, S.; Garcia, G.; Soldi-Lose, H.; de Miranda, B. K. C.; Alcaraz, C.; Carrasco, N.; Pernot, P.; et al. Determination of the absolute photoionization cross sections of CH_3 and I produced from a pyrolysis source, by combined synchrotron and vacuum ultraviolet laser studies. *J. Phys. Chem. A* **2010**, *114* (9), 3237−3246.
(35) Taatjes, C. A.; Osborn, D. L.; Selby, T. M.; Meloni, G.; Fan, H.; Pratt, S. T. Absolute photoionization cross-section of the methyl radical. *J. Phys. Chem. A* **2008**, *112* (39), 9336−9343.
(36) Savee, J. D.; Soorkia, S.; Welz, O.; Selby, T. M.; Taatjes, C. A.; Osborn, D. L. Absolute photoionization cross-section of the propargyl radical. *J. Chem. Phys.* **2012**, *136* (13), 134307.
(37) Wang, J.; Yang, B.; Cool, T. A.; Hansen, N.; Kasper, T. Near-threshold absolute photoionization cross-sections of some reaction intermediates in combustion. *Int. J. Mass Spectrom.* **2008**, *269* (3), 210−220.
(38) Kameta, K.; Kouchi, N.; Ukai, M.; Hatano, Y. Photoabsorption, photoionization, and neutral-dissociation cross sections of simple hydrocarbons in the vacuum ultraviolet range. *J. Electron Spectrosc. Relat. Phenom.* **2002**, *123* (2−3), 225−238.
(39) Samson, J. A. R.; Haddad, G. N.; Masuoka, T.; Pareek, P. N.; Kilcoyne, D. A. L. Ionization yields, total absorption, and dissociative photoionization cross sections of CH_4 from 110 to 950 Å. *J. Chem. Phys.* **1989**, *90* (12), 6925−6932.
(40) Cool, T. A.; McIlroy, A.; Qi, F.; Westmoreland, P. R.; Poisson, L.; Peterka, D. S.; Ahmed, M. Photoionization mass spectrometer for studies of flame chemistry with a synchrotron light source. *Rev. Sci. Instrum.* **2005**, *76* (9), 094102.
(41) Hatano, Y. Interaction of photons with molecules − cross-sections for photoabsorption, photoionization, and photodissociation. *Radiat. Environ. Biophys.* **1999**, *38* (4), 239−247.
(42) Person, J. C.; Nicole, P. P. Isotope effects in the photoionization yields and the absorption cross sections for acetylene, propyne, and propene. *J. Chem. Phys.* **1970**, *53* (5), 1767−1774.
(43) Holland, D. M. P.; Shaw, D. A.; Hayes, M. A.; Shpinkova, L. G.; Rennie, E. E.; Karlsson, L.; Baltzer, P.; Wannberg, B. A photo-absorption, photodissociation and photoelectron spectroscopy study of C_2H_4 and C_2D_4. *Chem. Phys.* **1997**, *219* (1), 91−116.
(44) Person, J. C.; Nicole, P. P. Isotope effects in the photoionization yields and the absorption cross sections for ethylene and n-butane. *J. Chem. Phys.* **1968**, *49*, 5421−5437.

DOI: 10.1021/acs.jpca.6b06634
J. Phys. Chem. A 2016, 120, 7890−7901

(45) Dodson, L. G.; Shen, L.; Savee, J. D.; Eddingsaas, N. C.; Welz, O.; Taatjes, C. A.; Osborn, D. L.; Sander, S. P.; Okumura, M. VUV photoionization cross sections of HO_2, H_2O_2, and H_2CO. *J. Phys. Chem. A* **2015**, *119* (8), 1279−1291.
(46) Cooper, G.; Anderson, J. E.; Brion, C. E. Absolute photoabsorption and photoionization of formaldehyde in the VUV and soft X-ray regions (3−200 eV). *Chem. Phys.* **1996**, *209* (1), 61−77.
(47) Cool, T. A.; Wang, J.; Nakajima, K.; Taatjes, C. A.; McIlroy, A. Photoionization cross sections for reaction intermediates in hydrocarbon combustion. *Int. J. Mass Spectrom.* **2005**, *247* (1−3), 18−27.
(48) Yang, B.; Wang, J.; Cool, T. A.; Hansen, N.; Skeen, S.; Osborn, D. L. Absolute photoionization cross-sections of some combustion intermediates. *Int. J. Mass Spectrom.* **2012**, *309*, 118−128.
(49) Cool, T. A.; Nakajima, K.; Mostefaoui, T. A.; Qi, F.; McIlroy, A.; Westmoreland, P. R.; Law, M. E.; Poisson, L.; Peterka, D. S.; Ahmed, M. Selective detection of isomers with photoionization mass spectrometry for studies of hydrocarbon flame chemistry. *J. Chem. Phys.* **2003**, *119* (16), 8356−8365.
(50) Holland, D. M. P.; Shaw, D. A. A study of the valence-shell photoabsorption, photodissociation and photoionisation cross-sections of allene. *Chem. Phys.* **1999**, *243* (3), 333−339.
(51) Wang, J.; Yang, B.; Cool, T. A.; Hansen, N. Absolute cross-sections for dissociative photoionization of some small esters. *Int. J. Mass Spectrom.* **2010**, *292* (1−3), 14−22.
(52) Au, J. W.; Cooper, G.; Brion, C. E. The molecular and dissociative photoionization of ethane, propane, and n-butane: absolute oscillator strengths (10−80 eV) and breakdown pathways. *Chem. Phys.* **1993**, *173* (2), 241−265.
(53) Kurimoto, N.; Brumfield, B.; Yang, X.; Wada, T.; Diévart, P.; Wysocki, G.; Ju, Y. Quantitative measurements of HO_2/H_2O_2 and intermediate species in low and intermediate temperature oxidation of dimethyl ether. *Proc. Combust. Inst.* **2015**, *35* (1), 457−464.
(54) Le Tan, N. L.; Djehiche, M.; Jain, C. D.; Dagaut, P.; Dayma, G. Quantification of HO_2 and other products of dimethyl ether oxidation (H_2O_2, H_2O, and CH_2O) in a jet-stirred reactor at elevated temperatures by low-pressure sampling and continuous-wave cavity ring-down spectroscopy. *Fuel* **2015**, *158*, 248−252.
(55) Guo, H.; Sun, W.; Haas, F. M.; Farouk, T.; Dryer, F. L.; Ju, Y. Measurements of H_2O_2 in low temperature dimethyl ether oxidation. *Proc. Combust. Inst.* **2013**, *34* (1), 573−581.
(56) Herrmann, F.; Jochim, B.; Oßwald, P.; Cai, L.; Pitsch, H.; Kohse-Höinghaus, K. Experimental and numerical low-temperature oxidation study of ethanol and dimethyl ether. *Combust. Flame* **2014**, *161* (2), 384−397.
(57) Liu, I.; Cant, N. W.; Bromly, J. H.; Barnes, F. J.; Nelson, P. F.; Haynes, B. S. Formate species in the low-temperature oxidation of dimethyl ether. *Chemosphere* **2001**, *42* (5−7), 583−589.
(58) Sztáray, B., personal communication 2015.

DOI: 10.1021/acs.jpca.6b06634
J. Phys. Chem. A 2016, 120, 7890−7901